

Original article

Multi-scale comprehensive study of the dynamic evolution of permeability during hydrate dissociation in clayey silt hydrate-bearing sediments

Yaobin Li^{1,2}, Tianfu Xu^{1,2}, Xin Xin^{1,2}^{*}, Yingli Xia³, Huixing Zhu^{1,2}, Yilong Yuan^{1,2}

¹Key Laboratory of Groundwater Resources and Environment, Ministry of Education, Jilin University, Changchun 130021, P. R. China

²Jilin Provincial Key Laboratory of Water Resources and Environment, Jilin University, Changchun 130021, P. R. China

³College of Water & Architectural Engineering, Shihezi University, Shihezi 832000, P. R. China

Keywords:

Permeability
clayey silt hydrate reservoir
multi-scale
hydrate decomposition

Cited as:

Li, Y., Xu, T., Xin, X., Xia, Y., Zhu, H., Yuan, Y. Multi-scale comprehensive study of the dynamic evolution of permeability during hydrate dissociation in clayey silt hydrate-bearing sediments. *Advances in Geo-Energy Research*, 2024, 12(2): 127-140.

<https://doi.org/10.46690/ager.2024.05.05>

Abstract:

The exploitation of natural gas hydrates is in essence the process of hydrate dissociation from the solid phase into the gas and liquid phases, which is a complex problem involving phase transition and gas-water multi-phase flow. Permeability is a useful parameter for characterizing the flow capacity of sediments, and the pore-structure changes caused by hydrate dissociation make this parameter characterized by spatial and temporal evolution. Clayey silt sediments form the hydrate accumulation reservoir in the South China Sea, whose lithological characteristics (shallow buried deep, poor permeability, and low cementation) are unfavorable to fluid flow, leading to difficulties in the production prediction of clayey silt hydrate-bearing sediments. In this paper, the mutual feed-back mechanism between pore-structure and permeability during hydrate dissociation was clarified using the lattice Boltzmann model method. Core-scale seepage experiments were carried out to validate the dynamic evolution of permeability relationship. The permeability calculation module of Tough+Hydrate code was developed to quantitatively describe the evolution of this relationship, and the first hydrate production test in the Shenhu area was evaluated to validate the applicability of pore- and core-scale study at the site scale. This study clarifies the dynamic evolution mechanism of permeability during hydrate dissociation, and establishes a permeability evolution model in a S-shape suitable for clayey silt hydrate-bearing sediments.

1. Introduction

Natural gas hydrates (NGH) are generally considered as an important potential future energy resource (Sloan, 2003; Tian et al., 2024), which could be used during the transition of the energy system from the existing fossil energy to commercial renewable energy (Chu et al., 2023; Lu et al., 2023; Olga et al., 2023). The production methods and technologies of NGH are gradually becoming more mature, while they are still a long way away from the stage of “commercial production.” There is still an order of magnitude difference between the productivity obtained from hydrate production test and the minimum standard (the sea area, 5.0×10^5 m³/d; the permafrost area,

3.0×10^3 m³/d) for commercial production (Wu et al., 2020).

Thus far, ten production tests have been carried out in Canada, the United States, Japan, and China, successively (Uddin et al., 2014; Yamamoto et al., 2019; Ye et al., 2020; Gajanan et al., 2024). The encountered problems include serious sand blockage (Uchida et al., 2019) and significant land subsidence (Yakushev, 2023), which are caused by the change in the pore-structure of sediments due to hydrate phase transition. From the productivity point of view, completed NGH production tests suffer from low daily gas production (Yoshimoto et al., 2023) and insufficient stable-production period (Pratama et al., 2023). It can be seen that the key

problem limiting the productivity increase in production test is that existing studies are unclear about the hydrate phase transition and fluid flow processes during NGH production in hydrate-bearing sediments (HBS) (Lu et al., 2023).

Unlike conventional oil-gas resources, NGH are trapped in solid form in the pore space of seafloor unconsolidated sediment (Boswell et al., 2022; Moridis et al., 2023). The exploitation of hydrates by means of depressurization, injecting heat, or injecting inhibitors is based on the process of hydrate dissociation from the solid phase into the gas and liquid phases. This is a complex problem involving phase transition and gas-water multi-phase flow (Anderson et al., 2014; Mahmood and Guo, 2023). The pore structure changes caused by hydrate dissociation directly affect the permeability evolution and can be considered a typical dynamic parameter with spatial and temporal evolution. Therefore, quantitatively describing the dynamic evolution of permeability during hydrate dissociation is an urgent challenge in the prediction of recovery and the environmental impact assessment of the NGH production process (Cai et al., 2020b).

Sandy hydrate-bearing sediments exhibit favorable permeability and high hydrate saturation, while clayey silt hydrate-bearing sediments have good stratification, poor permeability, and high irreducible water saturation, which leads to obvious differences in seepage characteristics between them. Hydrates in these two types of sediment are also fundamentally different in their occurrence patterns and decomposition behaviors (Shunsuke et al., 2023). Clayey silt sediments in the South China Sea (SCS) form a hydrate accumulation reservoir, whose lithological characteristics are unfavorable to gas-water production and fluid flow, such as shallow buried depth, poor permeability, and low cementation. These factors lead to difficulties in production prediction for clayey silt hydrate-bearing sediments (Li et al., 2018). Therefore, regarding practical applications, this study focuses on the dynamic evolution of permeability during hydrate dissociation in clayey silt hydrate-bearing sediments.

A single-scale physical mechanism is insufficient to describe the complex phenomena of the hydrate dissociation system. Micro-scale studies could clarify the physical process of the dynamic evolution of pore-structure and fluid flow, but if the physical quantities derived from pore-scale calculations cannot be transferred to the core and site scale, the physical characteristics of the system as a whole will not be accurately understood (Wang et al., 2023). Consequently, it is necessary to combine multiple scales, such as micro-scale characterization, core-scale laboratory seepage experiments, and site-scale production test, to comprehensively study the dynamic evolution of permeability during hydrate dissociation.

In recent years, researchers at home and abroad have put considerable effort into clarifying the dynamic evolution of permeability during hydrate dissociation at different scales. On the pore scale, some micro-simulation methods, such as pore network model, lattice Boltzmann model (LBM), and Monte Carlo method, were used to describe the hydrate formation and dissociation process (Ji et al., 2017; Abdoli et al., 2018), and to qualitatively calculate the effects of different factors on the permeability of porous media during hydrate

dissociation (Yang et al., 2022; Wu et al., 2023; Yamaguchi et al., 2023; Wang et al., 2024). At the core scale, hydrates were synthesized in quartz sands with different particle sizes, the permeability of the quartz sands at different hydrate saturation was measured, and the evolution of the relationship between permeability and hydrate saturation was obtained (Li et al., 2019; Shen et al., 2020; Lei et al., 2021; Cheng et al., 2023). At the site scale, according to the geological and engineering conditions of the actual hydrate production area, taking into account the geological structure conditions and the heterogeneity of hydrate saturation, the production processes of hydrate production tests were reproduced, and the long-term hydrate production has been predicted by the Tough+Hydrate code (Vedachalam et al., 2019; Yu et al., 2019; Myshakin et al., 2022). In addition, seepage experiments of hydrate-bearing sediments samples were conducted, which combined concurrent imaging by X-ray CT to study the dynamic evolution of permeability (Chen et al., 2018; Cai et al., 2020a; Zhao et al., 2023).

However, with the continuous deepening of research, some problems still need to be solved:

- 1) Lack of consideration of the complex pore-structure of clayey silt sediments in the research of the dynamic evolution relationship between permeability and pore structure during hydrate dissociation;
- 2) Studies based on the core-scale seepage experiments have difficulties in clarifying the pore-structure evolution of sediments during hydrate dissociation, and need to be preceded by characterizing the hydrate phase transition on the pore-scale;
- 3) Most pore-scale simulation and core-scale experimental results fail to perform validation against observations from site-scale hydrate production tests.

To address the above problems, this study focused on the dynamic evolution of permeability during hydrate dissociation in clayey silt hydrate-bearing sediments based on the actual geological conditions of hydrate accumulation area in the SCS. In response to this scientific challenge, the mutual feed-back mechanism between pore-structure and permeability during hydrate dissociation was clarified using the LBM method, and core-scale seepage experiments were carried out to validate the dynamic evolution relationship of permeability. The permeability calculation module of Tough+Hydrate code was developed to quantitatively describe the evolution of this relationship, and the first hydrate production test in the Shenhu area was taken to validate the applicability of pore- and core-scale study at the site scale. This study clarifies the dynamic evolution mechanism of permeability during hydrate dissociation and establishes the permeability evolution model suitable for clayey silt hydrate-bearing sediments, providing theoretical guidance for the future commercial production of NGH in China.

2. Permeability model establishment

2.1 Pore-scale permeability evolution mechanism

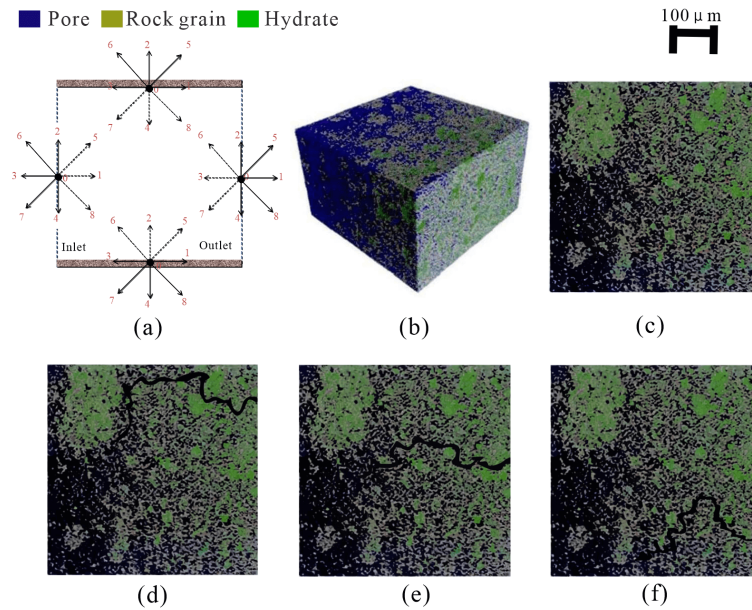


Fig. 1. Pore-scale LBM model of the clayey silt hydrate-bearing sediment setup. (a) Boundary conditions; (b) 3-D pore structure (Li, 2020); (c) 2-D pore structure; (d) A-type pore structure of the simulation setup; (e) B-type pore structure of the simulation setup and (f) C-type pore structure of the simulation setup.

2.1.1 Model systems

The LBM was used to study the dynamic evolution of permeability during hydrate dissociation at the pore scale. The basic idea of the LBM method is to fully discretize the time and space in which the fluid exists, and to calculate the fluid flow process through the migration and collision of the distribution function of particles on the lattice points (Fuji et al., 2020).

On the two-dimensions (2-D) LBM model, mass transfer, heat transfer and NGH dissociation kinetic models were supplemented to characterize the hydrate phase transition, where the mass transfer process is considered only in the liquid phase and is solved at the gas-water interface by Henry's law; hydrate dissociation absorbs heat all the time and obeys Kim's model (Hamid and Christian, 2015; Prasad and Sangwai, 2023; Pratama et al., 2023).

2.1.2 Model setup

(i) Conceptual model

The D2Q9 model, which is most commonly used in solving fluid flow process, was used to study the dynamic evolution mechanism of permeability during hydrate dissociation in hydrate-bearing sediments. After comprehensively considering the description accuracy and the computational efficiency, a LBM system with 500×500 (X, Y) grids was constructed. In this system, the upper and lower boundary and the rock particle surface were solid phase, which was set as a bounce-back scheme. This boundary condition was simple in form, easy to compute, and suitable for describing irregular boundaries. The lateral boundary was set as a hydrodynamic scheme (Zou-He scheme), in which a constant value of pressure or velocity is assigned to the boundary to provide a driving force for fluid

flow (Fig. 1(a)).

Fig. 1(b) shows the microscopic pore-structure of the clayey silt hydrate-bearing sediment samples obtained from the Shenhu Sea. The D2Q9 model used for this study was 2-D. It should be noted that pores were generally incompletely connected in the 2-D core section (Fig. 1(c)), that is, the permeability of sediments could not be measured before the extensive dissociation of the hydrate. Therefore, it is necessary to carve the control seepage channel on the 2-D pore structure according to the characterization of three-dimensions (3-D) pore structure and fluid flow (Fig. 1(b)). Finally, as shown in Figs. 1(d)-1(f), three clayey silt hydrate-bearing sediments with different initial pore structure were designed.

(ii) Determination of parameters

In the designed system, the initial macroscopic velocity and density of the fluid was 0 cm/s and 1 g/cm^3 , respectively, and the pressure difference between the two lateral boundaries was $6.0 \times 10^{-7} \text{ Pa/cm}$.

To characterize the clayey silt hydrate-bearing sediments, the initial spatial distribution of hydrate and rock particles were given with reference to the hydrate-bearing core sample from the Shenhu area in the SCS.

The length of the LBM system was only $500 \mu\text{m}$, and the initial temperature and pressure distributions within the hydrate-bearing sediments were hardly affected by the geothermal gradient and hydrostatic pressure. Thus, the initial temperature and pressure values within the entire LBM grids system were set to $13.6 \text{ }^\circ\text{C}$ and 13.4 MPa , respectively, under which conditions the hydrate could stably exist (Li et al., 2023a).

(iii) Simulation scheme

In order to establish a mathematical equation accurately describing the dynamic evolution relationship between permeability and hydrate saturation during hydrate dissociation, the

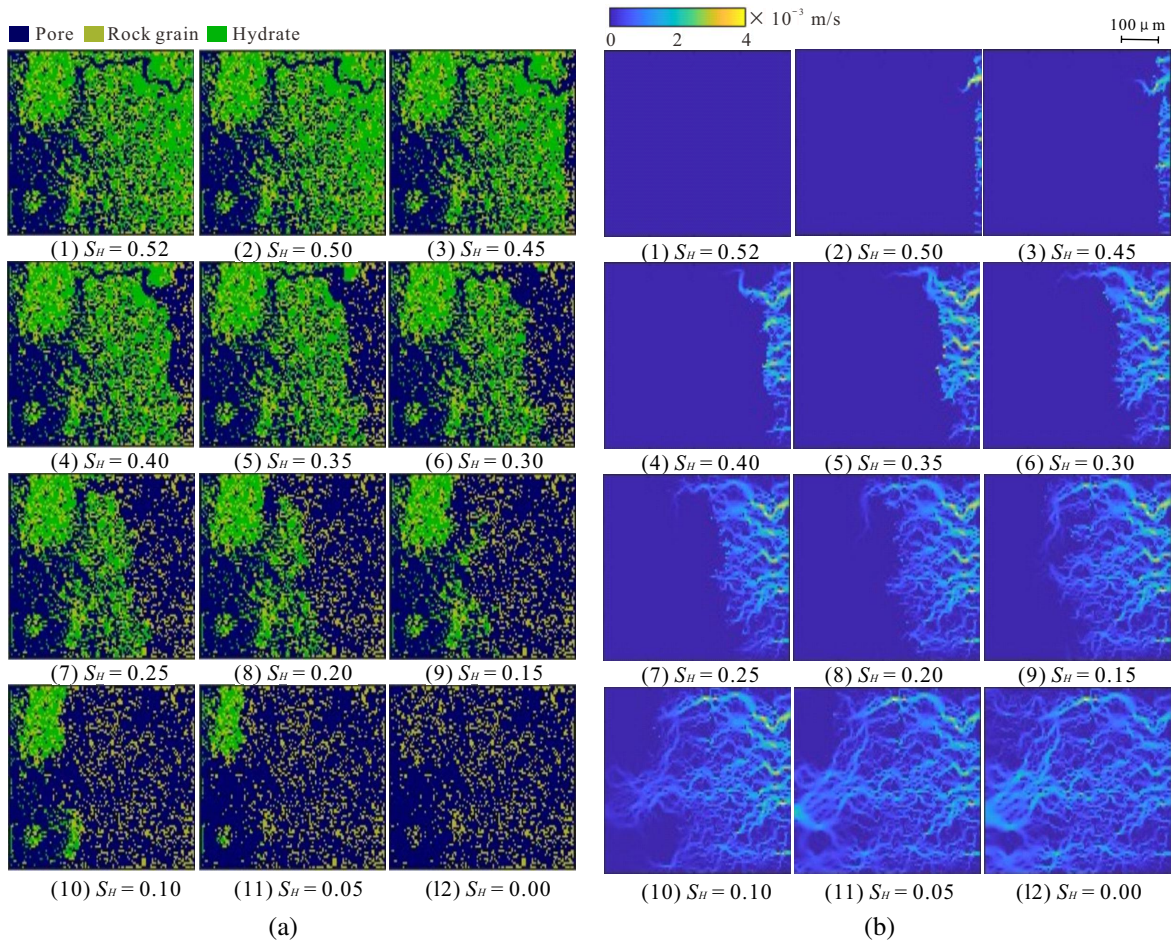


Fig. 2. Pore-scale hydrate dissociation in sediments with A-type pore structure. (a) Pore structure evolution and (b) seepage field evolution.

evolution of pore structure in three types of sediments under depressurization were studied ($S_H = 0.52, 0.51, 0.50, \dots, 0.01, 0.00$, 53 hydrate dissociation schemes). Then, the permeability in the sediments corresponding to different hydrate saturation were measured ($S_H = 0.52, 0.51, 0.50, \dots, 0.01, 0.00$, 53 flow schemes).

2.1.3 Simulation results

(i) Evolution of pore structure

The right boundary was set at constant low-pressure to simulate depressurization wells. The length of LBM system was small, and the depressurization amplitude was set to 0.3 MPa to avoid the unclear evolution of pore structure in the clayey silt sediments caused by the rapid dissociation of hydrate.

The pore structure and seepage field evolution during hydrate dissociation in sediments with A-type pore structure were shown in Fig. 2. In the early stage of depressurization, the hydrate dissociation behavior occurred mainly near the low-pressure boundary ($0.52 \rightarrow 0.45$). With the progress of depressurization, the pressure drop was transferred at different rates in different sediments areas, and the rate of thermal convection within the control seepage channel was much greater than of

thermal conduction across the primary rock particles. As a result, the hydrate dissociation regions gradually developed differences. This phenomenon was reflected in the figures, where the hydrate dissociation behavior occurs firstly near the control seepage channel with connectivity and progressively unfolds around the control seepage channel with continued depressurization ($0.45 \rightarrow 0.00$).

(ii) Permeability evolution

The primary key parameter to characterize the fluid flow capacity of sediments is absolute permeability, which depends solely on the sediment characteristics. According to the different hydrate states of the sediments, absolute permeability could be classified as follows: Effective permeability $k(S_H)$: Absolute permeability of sediments with hydrate; and intrinsic permeability k_0 : Absolute permeability of sediments without hydrate.

The fluid flow capacity of the sediments varies from region to region and even from site to site in the same region, so there is no practical significance in studying the dynamic evolution of effective permeability alone. Therefore, the normalized permeability k_{nor} was used to characterize the dynamic evolution of absolute permeability during hydrate dissociation, to make the datasets comparable to each other while maintaining their

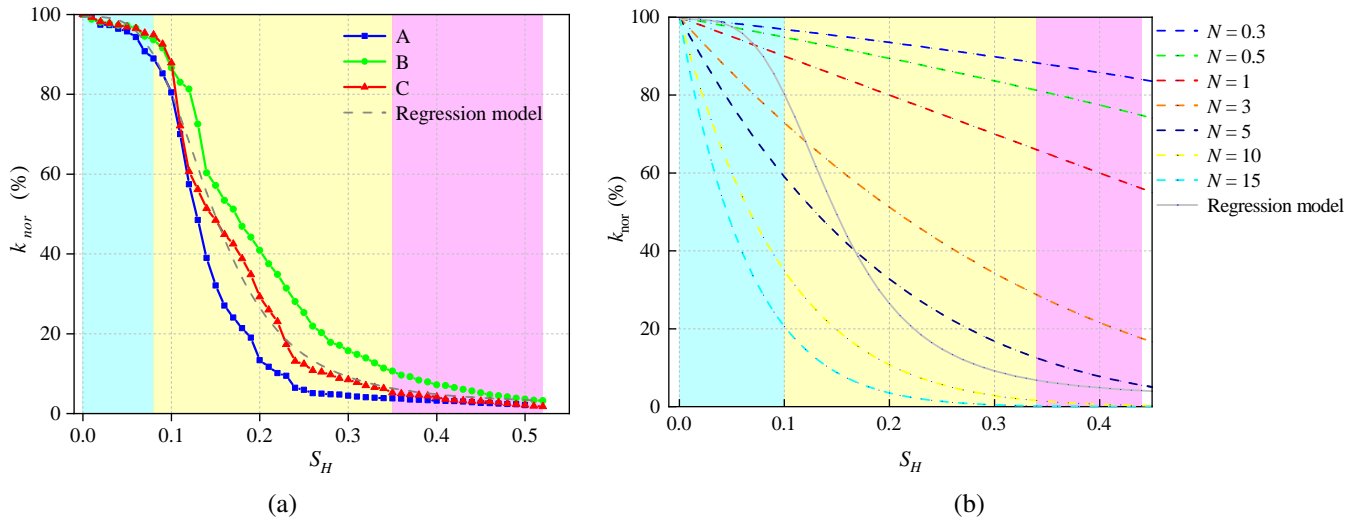


Fig. 3. Evolution of permeability during hydrate dissociation. pink area-early stage of hydrate dissociation; light yellow area-developing stage of hydrate dissociation; light blue area-decaying stage of hydrate dissociation. (a) Normalized permeability; (b) comparison of the regression model and the Masuda mode.

internal statistical relationship:

$$k_{nor} = \frac{k(S_H)}{k_0} \quad (1)$$

According to the simulation results, the dynamic evolution of normalized permeability (k_{nor}) during hydrate dissociation in the sediments were plotted in Fig. 3. It could be found that the hydrate dissociation improves permeability.

Combining the pore structure evolution during hydrate dissociation (Fig. 2(a)) in the different sediments, the dynamic evolution of permeability during hydrate dissociation in clayey silt hydrate-bearing sediments could be divided into three stages:

- 1) Early stage of hydrate dissociation ($0.52 \rightarrow 0.35$): The hydrate dissociation behavior occurred mainly near the depressurization wells and control seepage channel. Due to the large amount of hydrate dissociation, the fluid flow capacity of the right-side region of the sediments was enhanced. However, the dissociation behavior occurred only in the local regions, so the permeability growth of the whole sediments was limited. Moreover, the evolution trend of k_{nor} was similar to that of $k(S_H)$, with a relatively smooth growth.
- 2) Developing stage of hydrate dissociation ($0.35 \rightarrow 0.08$): With the progress of depressurization, particle-filled hydrates in the sediments begin to dissociate in large quantities, and the slope of the $k(S_H)$ evolution curve at this stage is the largest. Many enriched hydrates in pore throats or small pore channels dissociate, as presented in Fig. 3(a). The slope of the $k(S_H)$ and k_{nor} evolution curve approaches 90 degrees at a particular hydrate saturation, which greatly improves the permeability growth of the whole sediments. Thus, the k_{nor} of the sediments increase rapidly with hydrate dissociation. However, because the sediments exhibit differences in pore structure, control

seepage channel and hydrate distribution, at this stage, the evolution trend of k_{nor} in different sediments still have some differences in the specific rate while maintaining the same general trend.

- 3) Decaying stage of hydrate dissociation ($0.08 \rightarrow 0.00$): Particle-filled hydrates have been essentially dissociated, and particle-encapsulated hydrates away from the control seepage channel dissociate in this stage. These small amounts of residual hydrates affect the fluid flow capacity of the sediments mainly by influencing the hydraulic tortuosity and pore diameter of seepage channels, and exerting less effect on the pore throats size, also making the slope of the $k(S_H)$ evolution curve at this stage less steep. This is also in line with existing studies: Compared with particle-encapsulated hydrates, the occurrence of pore-filled hydrate has a greater effect on the effective permeability of sediments (Katagiri et al., 2017).

In order to quantitatively describe the pore-scale dynamic evolution of pore structure and permeability during hydrate dissociation in clayey silt hydrate-bearing sediments, this study establishes a mathematical equation describing the evolution relationship between normalized permeability (k_{nor}) and hydrate saturation (S_H) during hydrate dissociation in sediments:

$$k_{nor}(\%) = \frac{k(S_H)}{k_0} = 2.28826 + \frac{97.19184}{1 + \left(\frac{S_H}{0.14732}\right)^{3.61664}} \quad (2)$$

The curve of regression model was shown in Fig. 3(a). The R-squared (R^2) value was chosen to evaluate the fitting effect of the mathematical regression model with the micro-simulation data. The R^2 values were between [0,1], and the larger R^2 , the better fitting effect. The R^2 of the regression model was 0.973, so the mathematical equation obtained from the logistic regression analysis could greatly explain the pore-scale evolution relationship between permeability and hydrate

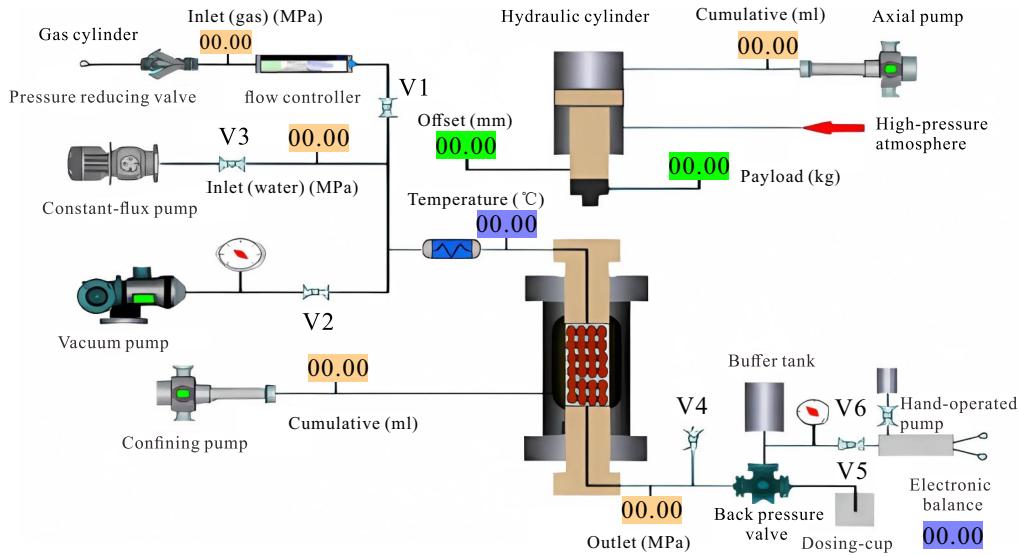


Fig. 4. Schematic of the multi-phase seepage experiment.

saturation during hydrate dissociation in the hydrate-bearing sediments.

To illustrate the physical significance of the regression model, it was compared with the Masuda model, which is currently the most commonly used effective permeability evolution model:

$$k_{nor} = (1 - S_h)^N \quad (3)$$

where N represents the attenuation index of permeability; its values are different for different hydrate-bearing sediments and need to be determined by core seepage experiments.

The Masuda model has been widely used and optimized. Minagawa et al. (2005) fitted the permeability at different hydrate saturations and proposed a range of N values between 2.5 and 9.8; Hardwick and Mathias (2018) used improved estimates of the hydrate saturation in the model.

As shown in Fig. 3(b), compared with the Masuda model with a simple form, the regression model obtained from pore-scale simulation could describe the dynamic evolution of permeability during hydrate dissociation in sediments more flexibly. At the early stage of hydrate dissociation ($0.52 \rightarrow 0.35$), the change in permeability with decreased hydrate saturation was similar to the Masuda model with $N = 10$. At the developing stage of hydrate dissociation ($0.35 \rightarrow 0.08$), the change in permeability with hydrate saturation decreased was similar to the Masuda model with $N = 3$ or 5. At the decaying stage of hydrate dissociation ($0.08 \rightarrow 0.00$), the change in permeability with decreased hydrate saturation was similar to the Masuda model with $N = 0.3$. The empirical value of the Masuda model (N) was given based on the lithology, pore structure, and hydrate distribution characteristics of the sediments. This study optimized this value from a constant to a dynamic parameter that changes constantly with the hydrate saturation during hydrate dissociation. Subsequently, based on the research on the characteristics of the clayey silt hydrate-bearing sediments, a permeability evolution model suitable for the clayey silt hydrate-bearing sediments in the SCS was

proposed.

2.2 Core-scale permeability evolution comparison

2.2.1 Experimental system

Core-scale experimental validation was conducted to provide a link between the pore-scale mechanism study and site-scale practical application. The hydrate-bearing core with characteristic porosity and hydrate saturation was prepared according to the characteristics of the lithology and hydrate distribution of sediments in the SCS. On this basis, the seepage parameters of core without and during hydrate dissociation were measured by a self-developed seepage experimental system.

The working principle of the self-developed seepage experiment system was shown in Fig. 4. On this basis, the following procedures could be carried out sequentially: the preparation of a hydrate-bearing core that was closer to the actual lithology of the clayey silt hydrate-bearing sediment; intrinsic permeability measurement according to Darcy's law; hydrate synthesis by the excess gas method; effective permeability measurement according to Darcy's law; and hydrate dissociation by depressurization.

2.2.2 Main experimental procedure

(i) Hydrate-bearing core preparation

Based on the mineral composition and particle size gradation of sediments in the South China Sea, core samples could be divided into two groups: Core skeleton (80%) and clayey filler (20%). Quartz sand (200 mesh) was chosen to replace the core skeleton with large particle size. Illite (4,000 mesh) was selected to replace the clayey filler with small particle size. The two were evenly mixed, and appropriate distilled water was added followed by thorough stirring (the moisture content was set at 10%). The particles were compacted and shaped by using an electric stripper, and a hydrate-bearing

Table 1. Data of the permeability evolution experiment.

Scheme	P_1 (MPa)	P_2 (MPa)	V_1 (cm ³)	V_2 (cm ³)	S_H (%)	$k(S_H)$ (mD)	k_{ir} (%)
Formation	13.915	2.93	/	/	20.29	2.388	20.85
	/	/	0.00	256.97	18.19	4.199	36.67
	/	/	256.97	653.43	14.95	5.770	50.38
	/	/	653.43	936.09	12.64	7.531	65.76
Dissociation	/	/	936.09	1,321.55	9.49	8.687	75.86
	/	/	1,321.55	1,718.01	6.25	10.351	90.39
	/	/	1,718.01	2,114.47	3.05	10.886	95.06
	/	/	2,114.47	2,487.69	0.00	11.452	100

core was obtained that closely resembled the actual lithology of the clayey silt HBS.

(ii) Permeability measurement

By adjusting the constant-flux pump and the valve V3 used to control the water input, distilled water was injected into the high-pressure reaction column at a certain rate. When the electric balance was stable in a certain period, that is, the seepage exhibited steady flow, the pressure of inlet P_{in} and outlet P_{out} were recorded and the pressure difference between them could be calculated $\Delta P = P_{in} - P_{out}$. Furthermore, the permeability of core could be calculated based on the observed data and Darcy's law:

$$k = \frac{\mu QL}{A\Delta P} \quad (4)$$

where μ represents the dynamic viscosity of the distilled water, 1.175×10^{-3} Pa·s; Q represents the flow rate of flow rate, 5.0×10^{-8} m³/s; L represents the length of core sample, 0.1 m; A represents the cross sectional area of core, 0.0019635 m².

(iii) Hydrate synthesis

Methane gas hydrates were synthesized by the excess gas method. According to the state equation of ideal gas, the actual synthesized hydrate saturation could be calculated as:

$$S_H = \frac{(P_1 - P_2)V_G M_{CH_4}}{164 \times \phi AL \rho_{CH_4}^0 RT_l} \quad (5)$$

where P_1 and P_2 respectively represent the expected pressure before hydrate synthesis and equilibrium pressure after hydrate synthesis in the reaction column, Pa; V_G represents the volume of gas inside the core, m³; M_{CH_4} represents the molar mass of methane gas, 0.016 kg/mol; ϕ represents the core porosity, dimensionless; $\rho_{CH_4}^0$ represents the density of methane gas, 0.7174 kg/m³; R represents the ideal gas constant, 8.314 J/(K·mol); T_l is the low temperature required for hydrate synthesis, 274.15 K.

(iv) Hydrate dissociation

After synthesizing the hydrate-bearing core with highest hydrate saturation and measuring its effective permeability, the pressure inside the high-pressure reaction column was gradually reduced to make hydrate dissociate to reach a certain hydrate saturation level. In practice, the specific amount of

hydrate dissociation could be deduced inversely from the methane gas mass discharged by dissociation:

$$\Delta S_H = \frac{V_2 - V_1}{164\phi AL} \quad (6)$$

where V_1 and V_2 respectively represent the mass of discharged methane gas before and after hydrate dissociation under a single depressurization, m³.

2.2.3 Experimental scheme setup

In order to better study the multi-scale dynamic evolution of permeability, the core-scale experiment needs to be combined with pore-scale simulation, so we referred the experimental scheme setup to the site data of clayey silt hydrate-bearing sediments in the SCS.

According to the geological data of the research area, different porosities and hydrate saturations of the sediments were considered. Previous studies have shown that the average value of sediment porosity and hydrate saturation in the Shenhu Sea were 0.38 and 0.21, respectively (Li et al., 2023a). Accordingly, the experimental scheme was designed: A clayey silt core with a porosity of 0.38 was synthesized using 80% quartz sand (75 μ m) and 20% illite (3.75 μ m), and the hydrate saturation was set to 0.00, 0.03, 0.06, 0.09, 0.12, 0.15, 0.18 and 0.20, separately.

The intrinsic permeability and effective permeability of the core samples with different hydrate saturation were measured at the experimental temperature of 274.15 K. The intrinsic permeability of the core sample k_0 was 11.452 mD, and other experimental data were arranged in Table 1.

2.2.4 Comparative analysis

The experimental results of core-scale permeability evolution and the regression model of pore-scale permeability evolution were compared as shown in Fig. 5.

The R-squared value between the core-scale experimental results and the prediction data of the pore-scale regression model was calculated to be 0.966. The fitting effect between them was great, which indicated that the regression model used for describing the permeability dynamic evolution obtained by the pore-scale simulation could well explain the core-scale effective permeability evolution.

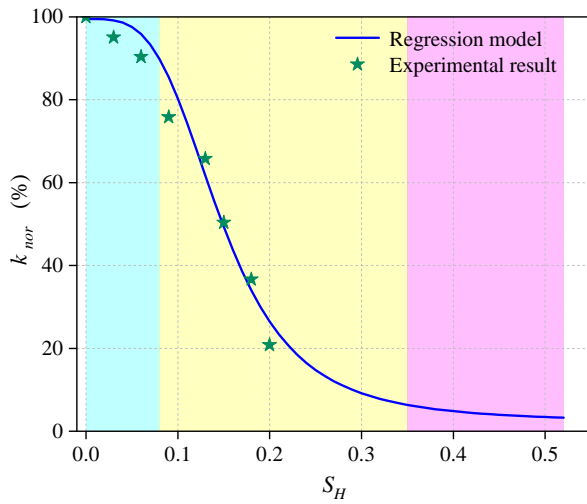


Fig. 5. Comparison of the experimental results of core-scale permeability evolution and the regression model of pore-scale permeability evolution. Pink area-early stage of hydrate dissociation; light yellow area-developing stage of hydrate dissociation; light blue area-decaying stage of hydrate dissociation.

It should be noted that, under the hydrate saturation range set by this study, the fitting effect between the pore-scale regression model and the core-scale experimental results was good at the developing stage of hydrate dissociation ($0.35 \rightarrow 0.08$), but the figures predicted by the regression model were slightly larger than the experimental results at the decaying stage of hydrate dissociation ($0.08 \rightarrow 0.00$). This is because in the pore-scale simulation, at the developing stage of hydrate dissociation, the particle-filled hydrates had been essentially dissociated, and mainly the particle-encapsulated hydrates away from the control seepage channel were subject to dissociation. These residual hydrates were small in amount and dispersed in distribution, so their dissociation had limited effects on the fluid flow capacity of the sediments. However, in the core-scale seepage experiment, on the one hand, the pressure of inlet was higher than the hydrate equilibrium pressure at the experimental temperature due to the driving pressure perturbation, which led to the localized distribution of hydrate and difficult dissociation; on the other hand, after the developing stage of hydrate dissociation, secondary hydrates were generated in the sediments due to the change in temperature and pressure conditions and methane gas distribution, which changed the hydrate distribution and pore structure in the sediments. Therefore, some differences were found between the pore- and core-scale permeability evolutions at the decaying stage of hydrate dissociation.

3. Permeability model programming and application

3.1 Model programming

3.1.1 Tough+Hydrate code

The Tough+Hydrate code (T+H) was developed by Lawrence Berkeley National Laboratory in the United States

based on the subsurface multi-phase seepage numerical simulation code TOUGH2 coupled with the natural gas hydrate formation and dissociation calculation module, which could be used to calculate the hydrate production process in the permafrost and sea area. Four phases (gas, liquid, hydrate, and ice) and four mass components (methane, water, hydrate, and inhibitors) were considered in the T+H code, and the equilibrium and kinetic models were used to describe the hydrate phase transition.

When calculating multi-phase fluid flow processes using the T+H code, it is necessary to establish the mass (or energy) conservation equations for each component (or energy) within the seepage system:

$$\frac{d}{dt} \int_{V_n} M^K dV = \int_{\Gamma_n} F^K \cdot n d\Gamma + \int_{V_n} q^K dV \quad (7)$$

where t represents the time, s; V_n represents the simulation element volume, m^3 ; Γ represents the simulation element surface area, m^2 ; M^K represents the mass (or energy) accumulation term of component K , kg/m^3 ; F^K represents the mass (or energy) flow term of component K , $kg/(m^2 \cdot s)$; n represents the unit normal vector, dimensionless; q^K represents the mass (or energy) source/sink term of component K , $kg/(m^3 \cdot s)$ (Moridis et al., 2008; Moridis, 2014; Li et al., 2023b).

3.1.2 Permeability calculation module

Based on the T+H code involving the coupling of Thermal (T)-Hydrological (H) field, the permeability calculation module was developed to quantitatively describe the dynamic evolution of permeability during hydrate dissociation in clayey silt sediments, which was then coupled to the T+H code.

The workflow of the permeability calculation module in the T+H code is shown in Fig. 6.

Hydrate dissociation (change in hydrate saturation) can impact the transportation space of fluids in the sediments (porosity), which further affects the transportation fluids ability of the sediments (permeability). The T+H v1.5 code being used regards the porous media as a serially connected bundle, and the evolution of permeability with porosity is calculated based on the series model and the preferential locations of hydrate dissociation:

$$k_{nor} = \frac{k(S_H)}{k_0} = \left(\frac{\varphi - \varphi_c}{\varphi_0 - \varphi_c} \right)^n \quad (8)$$

where φ_0 represents the porosity without hydrate, dimensionless; φ_c represents the critical porosity, dimensionless; n represents the attenuation index of permeability, which generally ranges from 5 to 29, and the higher the consolidation of sediments, the larger the n value will be (Li et al., 2023a).

The permeability calculation module in the T+H v1.5 code does not consider the complex particle morphology of clayey silt sediments and the effects of hydrate saturation on the permeability evolution during hydrate dissociation. Therefore, on the basis of the existing workflow, a module for calculating the dynamic evolution of permeability during hydrate dissociation in clayey silt sediments was developed and coupled to the Tough+Hydrate code.

The evolution of permeability during hydrate dissociation

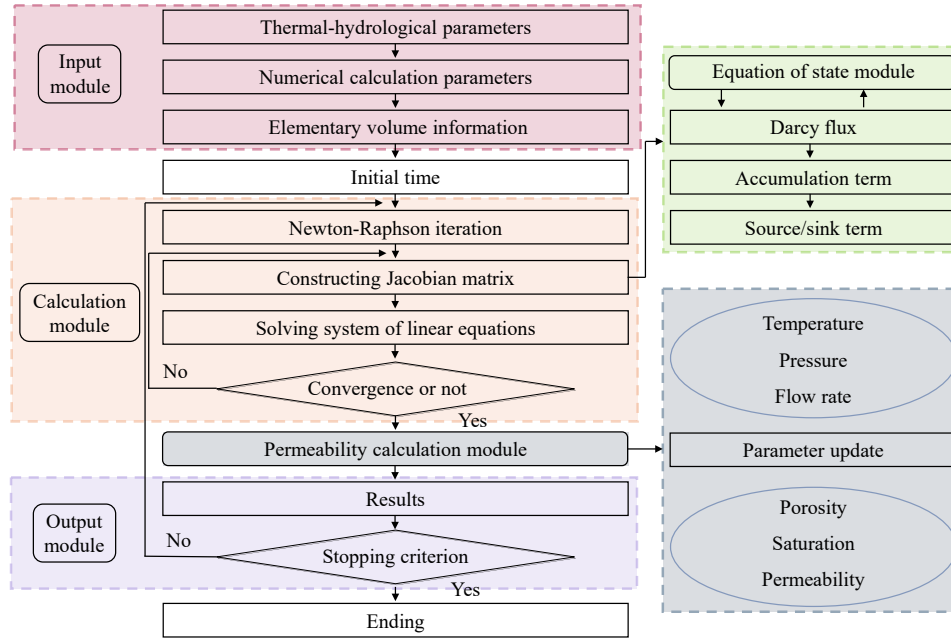


Fig. 6. Workflow of the permeability calculation module in the T+H code.

was related to the deformation degree of the sediment skeleton, which could be calculated in two stages:

- 1) The change in sediment porosity (ϕ) with the temperature and pressure evolution, which could be described by the pore compression coefficient in the existing T+H v1.5 code (Eq. (6)).
- 2) The change in sediment pore structure during hydrate dissociation, which could be described according to the permeability evolution model (Eq. (2)) obtained from the pore-scale mechanism simulation and the core-scale experimental validation:

$$\begin{aligned} \phi &= \phi_0 F_{PT} (1 - S_H) \\ F_{PT} &= \exp(\alpha_P \Delta P' + \alpha_T \Delta T) \end{aligned} \quad (9)$$

where F_{PT} is a function of porosity as a function of temperature and pressure; α_P represents the formation compression coefficient, dimensionless; α_T represents the thermal expansion coefficient of formation, dimensionless; $\Delta P'$ and ΔT are the difference between the pressure and temperature and the standard value, $\Delta P' = P - P_0$, $\Delta T = T - T_0$.

3.2 Site application

3.2.1 Geological background of the research area

As show in Fig. 7(a), the Shenhu area is located geologically in the Zhu II depression, Pearl River Mouth Basin, and geographically near the southeastern part of the Shenhu Shoal sea area in the SCS. The area topography is complex, with a general trend of low in the south and high in the north. A large number of landform units such as erosion flume, sea valley, sea mount, sea plateau, and submarine fan are developed in this area. Therefore, the Shenhu area has tectonic conditions for natural gas hydrate accumulation and is a key resource target area for hydrate exploration and production.

Since 2007, several hydrate drilling expeditions have been carried out in the Shenhu area: GMGS1 (2007), GMGS2 (2013), GMGS3 (2015), and GMGS4 (2016). As a result, the site characteristics of hydrate-bearing sediments and a large number of in-situ hydrate samples were obtained. A vertical well (SHSC-4) in 2017 and a horizontal well (SHSC2-6) in 2020 were set up to carry out hydrate depressurization productions; two successful hydrate production tests greatly advanced the natural gas hydrate research in China (Li et al., 2023b).

3.2.2 Model setup

In 2017, the China Geological Survey successfully carried out the first marine gas hydrate production tests in the Shenhu area. From the seismic reflection profiles (Fig. 7(b)), it could be seen that the production well (SHSC-4) is located in the middle of the southeastern continental slope of the Shenhu area, with a water depth of 1,266 m. The hydrate-bearing sediments system could be classified into three layers, the top to bottom (Li et al., 2018):

- 1) Hydrate layer (201-236 mbsf): Contains the hydrate and water (H+W), with an average porosity of 0.35, hydrate saturation of 0.34, and permeability of 2.9 mD;
- 2) Three-phase co-existence layer (236-251 mbsf): Contains the hydrate, free methane gas and water (H+G+W), with an average porosity of 0.33, hydrate saturation of 0.32, gas saturation of 0.16, and permeability of 1.5 mD, the water salinity linearly attenuates with the buried depth increasing;
- 3) Free gas layer (251-278 mbsf): Contains the free methane gas and water (G+W), with an average porosity of 0.32, gas saturation of 0.078 and permeability of 7.4 mD.

The lithology of all of the hydrate layer, three-phase co-

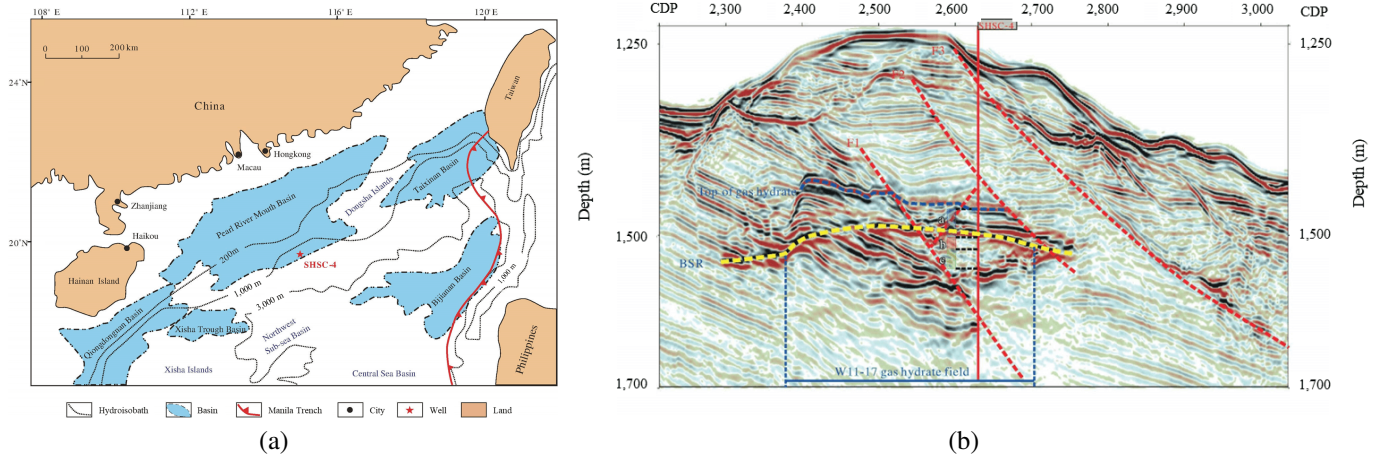


Fig. 7. Geological background in the research area. (a) Location of the Shenhu area in the SCS and (b) seismic reflection profiles of production well in the first marine gas hydrate production tests (Li et al., 2018).

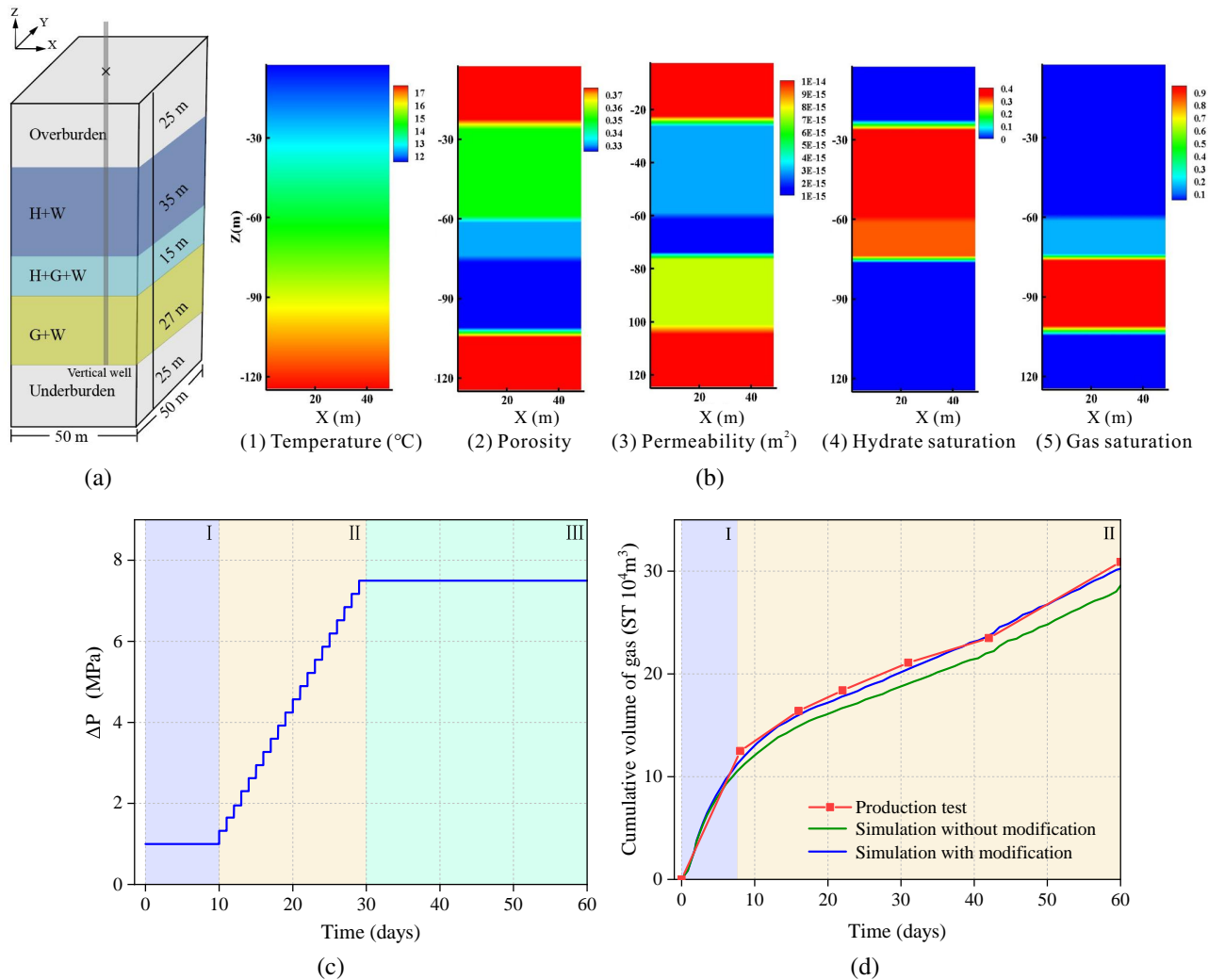


Fig. 8. Numerical simulation of the first marine gas hydrate production tests. (a) Conceptual hydrate production model; (b) initial condition; (c) simulation depressurization process and (d) comparison of gas production between the simulation results and the production test.

Table 2. Main parameters and sediment properties of the production model.

Subsystems	Parameter	Value	Parameter	Value
Hydrate + Water layer	Thickness (m)	35	Porosity (-)	0.35
	Permeability (mD)	2.9	Water saturation (-)	0.66
	Hydrate saturation (-)	0.34	Gas saturation (-)	0.00
Hydrate + Gas + Water layer	Thickness (m)	15	Porosity (-)	0.33
	Permeability (mD)	1.5	Water saturation (-)	0.53
	Hydrate saturation (-)	0.31	Gas saturation (-)	0.16
Gas + Water layer	Thickness (m)	37	Porosity (-)	0.32
	Permeability (mD)	7.4	Water saturation (-)	0.08
	Hydrate saturation (-)	0.00	Gas saturation (-)	0.92
	Water salinity (-)	0.033		
Overburden/underburden	Thickness (m)	25	Porosity (-)	0.38
	Permeability (mD)	10		
Hydrate properties	Rock grain density (kg/m ³)	2,600	Geothermal gradient (°C/100 m)	4.37
	Thermal conductivity (W/m/K)	0.50	Specific heat capacity (kJ/kg/K)	2.1

existence layer, and free gas layer is clayey silt.

Based on the above data, a hydrate production model of the Shenhu area was established (Fig. 8(a)), which comprised cuboids with dimensions of 50 m length \times 50 m width \times 127 m thickness. Along the X-coordinate and Y-coordinate, the mesh precision was 2.5 m, and 20 layers were equally divided; along the Z-coordinate, the mesh precision of hydrate layer, three-phase co-existence layer, and free gas layer was 1.5 m, the mesh precision of the overburden and underburden was 5.0 m, and 62 layers were divided. The whole hydrate production model was divided into $20 \times 20 \times 62 = 24,800$ grids.

As shown in Fig. 8(b), in the hydrate production model, the initial temperature gradually increased from the seafloor temperature (4.61 °C) based on the geothermal gradient (43.7 °C/km), and the initial pressure was calculated by the hydrostatic pressure. After calculation, the initial temperature and pressure at the bottom of the three-phase co-existence layer were 14.20 °C and 14.06 MPa, respectively, and the hydrate could exist under this situation. The main model parameters and sediment properties were given in Table 2.

The overburden and underburden with 30 m thickness were sufficient to characterize the temperature and pressure evolution during hydrate production, so the upper and lower boundary were set as constant pressure and temperature boundary where the fluid flow and heat exchange could occur. The lateral boundary was set to have no mass and heat flux. The vertical production well was laid in the middle of the clayey silt sediments ($X = 100$ m, $Y = 400$ m), which passes through the hydrate layer, three-phase co-existence layer, and free gas layer, which could be seen as an inner boundary with given pressure.

Table 3. Gas production comparison at key time nodes.

Time (d)	Production test (-)	Simulation without modification (-)	Simulation with modification (-)
8	12.5	11.25	12.04
16	16.1	15.04	16.13
22	18.4	16.66	17.79
31	21.1	17.21	20.72
42	23.5	21.83	23.61
60	30.9	28.03	30.13

3.2.3 Simulation results

As shown in Fig. 8(c), the depressurization process of the first marine gas hydrate production tests could be divided into three stages (Ning et al., 2020):

- 1) 0-10 d: The bottom-hole pressure rapidly reduced to about 13.5 MPa, stable production;
- 2) 10-30 d: The bottom-hole pressure gradually reduced to about 7.0 MPa;
- 3) 30-60 d: The bottom-hole pressure was maintained at 7.0 MPa, stable production.

According to the actual depressurization process, the first gas hydrate production tests of the Shenhu area were simulated by using the T+H code with and without the modified permeability calculation module, respectively. Gas production between the simulation results and the production test was compared in Fig. 8(d) and Table 3.

As can be seen from Fig. 8(d), compared with the T+H code without modification, the gas production data obtained

by the T+H code with the modified permeability calculation module were closer to those in the actual production test.

The difference between the two numerical simulation models is mainly reflected in the fact that the model with the modified permeability calculation module could more flexibly describe the dynamic evolution of permeability during hydrate dissociation. The pore-scale research results indicated that the permeability increased with the hydrate dissociation quicker in the model with modification compared with the model without modification.

Combined with the actual depressurization (Fig. 8(c)) and gas production (Fig. 8(d)) processes, the hydrate production process could be divided into two stages:

- 1) 0-7.6 d: In this stage, the gas production obtained by the simulation without modification and with modification was basically the same, and both fitted well with the production test data. This indicated that the permeability evolution within the two models was similar, that is, hydrate in the hydrate layer and three-phase co-existence layer basically did not dissociate under the small depressurization amplitude, and the obtained methane gas mainly came from the free gas in the three-phase co-existence layer and free gas layer. Therefore, the production rate of methane gas was larger in this stage, and gas production reached almost half of the total gas production.
- 2) 7.6-60 d: With the increase in depressurization amplitude, hydrate in the hydrate layer and three-phase co-existence layer underwent dissociation, and the permeability of the sediments gradually increased. The permeability increased with decreasing hydrate saturation quicker in the model with the modified permeability calculation module. On the one hand, the greater flow capacity led to the pressure-drop transmit and gas discharge quicker in the sediments, that is, the range of hydrate dissociation was larger in the same time period, and the discharge process of methane gas to production well was hindered. On the other hand, the discharge of free gas in the sediments meant that the average pressure of the sediments lowered, which made the actual pressure difference between the production well and the sediments larger and the hydrate dissociate quicker. Therefore, in this stage, the gas production calculated by the T+H code with the modified permeability calculation module was higher than that without the modified permeability calculation module and closer to that in the actual production test.

In summary, the simulation results obtained by using the T+H code with the modified permeability calculation module for the first marine gas hydrate production tests could well explain the evolution trend of the actual gas production process, and the permeability evolution model obtained from the pore-scale mechanism simulation and the core-scale experimental validation was suitable for calculating the depressurization production of actual clayey silt hydrate-bearing sediments.

4. Conclusions

This study focused on the dynamic evolution of permeability during hydrate dissociation in clayey silt hydrate-bearing sediments. The contributions of this work and some recommendations for future work can be given as follows:

- 1) Pore-scale mechanism study: On the basis of the LBM model, mass transfer, heat transfer and NGH dissociation kinetic models were supplemented to describe the hydrate phase transition to clarify the mutual feed-back mechanism between pore-structure and permeability during hydrate dissociation and to establish a mathematical equation describing the dynamic evolution of permeability.
- 2) Core-scale comparative study: A multi-phase seepage experiment system considering hydrate dissociation was designed. The hydrate-bearing core with characteristic porosity was prepared according to the characteristics of hydrate distribution and lithology of the sediments, and the permeability of core during hydrate dissociation were measured. Then, the pore- and core-scale results were compared to verify the applicability of the permeability evolution model suitable for the clayey silt hydrate-bearing sediments obtained in pore-scale simulation.
- 3) Programming of the permeability evolution model: On the basis of the T+H v1.5 code, a module for calculating the dynamic evolution of permeability during hydrate dissociation in clayey silt sediments was developed by replacing the previous series model with the permeability evolution model obtained from this research, and this module was coupled to the T+H code.
- 4) Site application of the permeability evolution model: Aimed at the area of hydrate production tests in the SCS, the production site (SHSC-4) was selected to establish the conceptual model and numerical simulation model of clayey silt hydrate-bearing sediments. The T+H code with and without the modified permeability calculation module was used to calculate the hydrate production process of the clayey silt sediments, and the gas production data were obtained. The simulation results and the production data of the first gas hydrate production tests in the SCS were fitted and compared, and the applicability of the permeability evolution model suitable for the clayey silt hydrate-bearing sediments was verified in an actual site.
- 5) We could establish that, in addition to change in the micro-pore structure of HBS caused by the dissociation of natural gas hydrate, which directly affect the permeability evolution, the dissociation of hydrate also deteriorates the HBS integrity and mechanical characteristics, which in turn affect the dynamic evolution of permeability. Thus, the geo-mechanical evolution during hydrate dissociation in sediments needs to be fully deciphered in future work.

Acknowledgements

This work was supported by the National Natural Science Foundation of China (Nos. 42276224 and 42206230), the Jilin Scientific and Technological Development Program (No. 20190303083SF), the International Cooperation Key Labo-

ratory of Underground Energy Development and Geological Restoration (No. YDZJ202102CXJD014), and the Graduate Innovation Fund of Jilin University (No. 2023CX100).

Conflict of interest

The authors declare no competing interest.

Open Access This article is distributed under the terms and conditions of the Creative Commons Attribution (CC BY-NC-ND) license, which permits unrestricted use, distribution, and reproduction in any medium, provided the original work is properly cited.

References

- Abdoli, S., Shafiei, S., Raof, A., et al. Insight into heterogeneity effects in methane hydrate dissociation via pore-scale modeling. *Transport in Porous Media*, 2018, 124: 183-201.
- Anderson, B., Boswell, R., Collett, T., et al. Review of the findings of the Ignik Sikurni CO₂-CH₄ gas hydrate exchange field trial. Paper Presented at 8th International Conference on Gas Hydrates, Beijing, China, 28 July-1 August, 2014.
- Boswell, R., Collett, T., Yamamoto, K., et al. Scientific results of the Hydrate-01 stratigraphic test well program, Western Prudhoe Bay Unit, Alaska North Slope. *Energy & Fuels*, 2022, 36(10): 5167-5184.
- Cai, J., Xia, Y., Lu, C., et al. Creeping microstructure and fractal permeability model of natural gas hydrate reservoir. *Marine and Petroleum Geology*, 2020a, 115: 104282.
- Cai, J., Xia, Y., Xu, S., et al. Advances in multiphase seepage characteristics of natural gas hydrate sediments. *Chinese Journal of Theoretical and Applied Mechanics*, 2020b, 52(1): 208-223. (in Chinese)
- Chen, X., Verma, R., Espinoza, D., et al. Pore-scale determination of gas relative permeability in hydrate-bearing sediments using X-ray computed micro-tomography and Lattice Boltzmann method. *Water Resources Research*, 2018, 54(1): 600-608.
- Cheng, F., Wu, Z., Su, X., et al. Compression-induced dynamic change in effective permeability of hydrate-bearing sediments during hydrate dissociation by depressurization. *Energy*, 2023, 264: 126137.
- Chu, H., Zhang, J., Zhang, L., et al. A new semi-analytical flow model for multi-branch well testing in natural gas hydrates. *Advances in Geo-Energy Research*, 2023, 7(3): 176-188.
- Fuji, T., Kamada, K., Sato, T., et al. Numerical simulation of crystal growth of CO₂ hydrate within microscopic Sand pores using phase field model for the estimation of effective permeability. *International Journal of Greenhouse Gas Control*, 2020, 95: 102960.
- Gajanan, K., Ranjith, P., Yang, S., et al. Advances in research and developments on natural gas hydrate extraction with gas exchange. *Renewable and Sustainable Energy Reviews*, 2024, 190: 114045.
- Hamid, K., Christian, H. Lattice Boltzmann formulation for conjugate heat transfer in heterogeneous media. *Physical Review E*, 2015, 91(2): 23304.
- Hardwick, J., Mathias, S. Masuda's sandstone core hydrate dissociation experiment revisited. *Chemical Engineering Science*, 2018, 175(1): 98-109.
- Ji, Y., Hou, J., Zhao, E., et al. Pore-scale study on methane hydrate formation and dissociation in a heterogeneous micromodel. *Journal of Natural Gas Science and Engineering*, 2017, 95: 104230.
- Katagiri, J., Konno, Y., Yoneda, J., et al. Pore-scale modeling of flow in particle packs containing grain-coating and pore-filling hydrates: Verification of a Kozeny-Carman-based permeability reduction model. *Journal of Natural Gas Science and Engineering*, 2017, 45: 537-551.
- Lei, X., Yao, Y., Luo, W., et al. Permeability change in hydrate-bearing sediments as a function of hydrate saturation: A theoretical and experimental study. *Journal of Petroleum Science and Engineering*, 2021, 208: 109449.
- Li, G., Li, X., Lv, Q., et al. Permeability measurements of quartz sands with methane hydrate. *Chemical Engineering Science*, 2019, 1: 1-5.
- Li, J., Ye, J., Qin, X., et al. The first offshore natural gas hydrate production test in South China Sea. *China Geology*, 2018, 1(1): 5-16.
- Li, X. Study on the on-board detection system and analysis methodology for natural gas hydrate core samples. Dalian, Dalian University of Technology, 2020. (in Chinese)
- Li, Y., Xin, X., Xu, T., et al. Study of multibranch wells for productivity increase in hydrate reservoirs based on a 3D heterogeneous geological model: A case in the Shenhu Area, South China Sea. *SPE Journal*, 2023a, 28(5): 2207-2222.
- Li, Y., Xu, T., Xin, X., et al. Sensitivity analysis of multiphase seepage parameters affecting the clayey silt hydrate reservoir productivity in the Shenhu Area. *Acta Geologica Sinica*, 2023b, 97(6): 1787-1800.
- Lu, C., Qin, X., Sun, J., et al. Research progress and scientific challenges in the depressurization exploitation mechanism of clayey-silt natural gas hydrates in the northern South China Sea. *Advances in Geo-Energy Research*, 2023, 10(1): 14-20.
- Mahmood, M., Guo, B. Gas production from marine gas hydrate reservoirs using geothermal-assisted depressurization method. *Advances in Geo-Energy Research*, 2023, 7(2): 90-98.
- Minagawa, H., Ohmura, R., Kamata, Y., et al. Water permeability measurements of gas hydrate-bearing sediments. Paper Presented at 5th International Conference on Gas Hydrates, Trondheim, Norway, 12-16 June, 2005.
- Moridis, G. User's manual for the hydrate v1.5 option of TOUGH+ v1.5: A code for the simulation of system behavior in hydrate-bearing geologic media. Berkeley, California: Lawrence Berkeley National Laboratory, 2014.
- Moridis, G., Kowalsky, M., Pruess, K., et al. Depressurization-induced gas production from Class 1 hydrate deposits. *SPE Reservoir Evaluation and Engineering*, 2008, 10(5): 458-481.
- Moridis, G., Kim, J., Reagan, M., et al. Analysis of short- and long-term system response during gas production from a

- gas hydrate deposit at the UBGH2-6 site of the Ulleung Basin in the Korean East Sea. *The Canadian Journal of Chemical Engineering*, 2023, 101(2): 735-763.
- Myshakin, E., Garapati, N., Seol, Y., et al. Numerical simulations of depressurization-induced gas hydrate reservoir (B1 Sand) response at the Prudhoe Bay Unit Kuparuk 7-11-12 Pad on the Alaska North Slope. *Energy & Fuels*, 2022, 36(5): 2542-2560.
- Ning, F., Liang, J., Wu, N., et al. Reservoir characteristics of natural gas hydrates in China. *Natural Gas Industry*, 2020, 40(8): 1-24. (in Chinese)
- Olga, G., Sergey, M., Vladimir, M., et al. Gas hydrates: applications and advantages. *Energies*, 2023, 16: 2866.
- Prasad, S., Sangwai, J. Impact of lighter alkanes on the formation and dissociation kinetics of methane hydrate in oil-in-water dispersions relevant for flow assurance. *Fuel*, 2023, 333(2): 126500.
- Pratama, M., Khan, H., Daigle, H., et al. A review of formation damage processes encountered during gas hydrate production. *Geoenergy Science and Engineering*, 2023, 228: 211958.
- Shen, S., Li, Y., Sun, X., et al. Experimental study on the permeability of methane hydrate-bearing sediments during triaxial loading. *Journal of Natural Gas Science and Engineering*, 2020, 82: 103510.
- Shunsuke, S., Zachary, M., Tomoya, N., et al. Simulations of hydrate reformation in the water production line of the second offshore methane hydrate production test in Japan's Nankai trough. *Fuel*, 2023, 349: 128606.
- Sloan, E. Fundamental principles and applications of natural gas hydrates. *Nature*, 2003, 426: 353-359.
- Tian, H., Liu, W., Ding, P., et al. Numerical simulation of elastic properties of hydrate-bearing sediments with digital rock technology. *Marine and Petroleum Geology*, 2024, 160: 106592.
- Uchida, S., Lin, J., Myshakin, E., et al. Numerical simulations of sand migration during gas production in hydrate-bearing sands interbedded with thin mud layers at site NGHP-02-16. *Marine and Petroleum Geology*, 2019, 108: 639-647.
- Uddin, M., Wright, F., Dallimore, S., et al. Gas hydrate dissociations in Mallik hydrate-bearing zones A, B, and C by depressurization: Effect of salinity and hydration number in hydrate dissociation. *Journal of Natural Gas Science and Engineering*, 2014, 21: 40-63.
- Vedachalam, N., Ramesh, S., Jyothi, V., et al. Numerical modeling of methane gas production from hydrate reservoir of Krishna Godhavari basin by depressurization. *Marine Georesources and Geotechnology*, 2019, 37(1-2): 14-42.
- Wang, H., Li, Y., Huang, L., et al. A pore-scale study on microstructure and permeability evolution of hydrate-bearing sediment during dissociation by depressurization. *Fuel*, 2024, 358: 130124.
- Wang, S., Catherine, S., Tom, B. Pore-scale imaging of multiphase flow fluctuations in continuum-scale samples. *Water Resources Research*, 2023, 59(6): e2023WR034720.
- Wu, N., Li, Y., Wan, Y., et al. Prospect of marine natural gas hydrate stimulation theory and technology system. *Natural Gas Industry*, 2020, 8(2): 173-187.
- Wu, P., Li, Y., Yu, T., et al. Microstructure evolution and dynamic permeability anisotropy during hydrate dissociation in sediment under stress state. *Energy*, 2023, 263: 126126.
- Yakushev, V. Environmental and technological problems for natural gas production in permafrost regions. *Energies*, 2023, 16(11): 4522.
- Yamaguchi, A., Sato, T., Tobase, T., et al. Multiscale numerical simulation of CO₂ hydrate storage using machine learning. *Fuel*, 2023, 334(2): 126678.
- Yamamoto, K., Wang, X., Tamak, M., et al. The second offshore production of methane hydrate in the Nankai Trough and gas production behavior from a heterogeneous methane hydrate reservoir. *RSC Advances*, 2019, 9: 25987-26013.
- Yang, J., Xu, Q., Liu, Z., et al. Pore-scale study of the multiphase methane hydrate dissociation dynamics and mechanisms in the sediment. *Chemical Engineering Journal*, 2022, 430(2): 132786.
- Ye, J., Qin, X., Xie, W., et al. The second natural gas hydrate production test in the South China Sea. *China Geology*, 2020, 2: 197-209.
- Yoshimoto, N., Wu, Q., Fujita, K., et al. Hydrate dissociation and mechanical properties of hydrate-bearing sediments under local thermal stimulation conditions. *Gas Science and Engineering*, 2023, 116: 205045.
- Yu, T., Guan, G., Abudula, A., et al. Gas recovery enhancement from methane hydrate reservoir in the Nankai Trough using vertical wells. *Energy*, 2019, 166: 834-844.
- Zhao, Z., Shou, Y., Zhou, X. Digital assessment of phase changes and heat transfer for hydrates in microstructures using X-ray CT imaging. *Geoenergy Science and Engineering*, 2023, 229: 212084.